Molecular modeling of the diffusion of ammonia through corrosion inhibitor films on copper

Agustin Salcedo, Stefano Caputo, Sophie Loehlé, Stephan N Steinmann, Carine Michel

Corrosion Science 240 (2024) 112491

Contents lists available at ScienceDirect

Corrosion Science

journal homepage: www.elsevier.com/locate/corsci

Molecular modeling of the diffusion of ammonia through corrosion inhibitor films on copper

Agustin Salcedo [a], Stefano Caputo [a], Sophie Loehlé [b], Stephan N. Steinmann [a], Carine Michel [a,*]

[a] CNRS, ENS de Lyon, LCH, UMR 5182, 69342, Lyon cedex 07, France
[b] TotalEnergies OneTech, 69360 Solaize, France

ARTICLE INFO

Keywords:
Corrosion
Ammonia
Copper
Molecular dynamics

ABSTRACT

Ammonia is emerging as a carbon-free fuel but its corrosive effect on metal engine components, particularly those made of copper and copper alloys, is a major concern to be addressed. Herein, typical corrosion inhibitors are investigated in the presence of NH_3. They have been ranked experimentally based on their corrosion initiation time while the NH_3 diffusion barrier through inhibitor films has been evaluated using molecular dynamics simulations using a classical force field that was tuned to improve the Cu/inhibitor interactions. The excellent agreement with experiments indicates that this simulation approach could allow for the screening of new corrosion inhibitors.

1. Introduction

The use of ammonia (NH_3) as an alternative carbon-free fuel in internal combustion engines (ICEs) is one of the most promising solutions for abating greenhouse gas emissions from transport and combating global warming [1–3]. NH_3 presents a larger energy density and is safer to handle than other alternative energy carriers such as H_2 [4], while also being commercially available worldwide due to its applications in the fertilizer industry. Furthermore, liquid ammonia can be kept at a reasonable temperature of −33 °C at standard pressure, or +20 °C at 9 bar, simplifying storage and transportation logistics compared to H_2 [5,6].

While conventional ICEs can operate on ammonia with minimal modifications such as adjustments to the compression ratio [7], a key concern arises from ammonia's potential to corrode metal parts of the engine. The electronegativity difference between nitrogen and hydrogen and the trigonal pyramidal asymmetrical shape give NH_3 a strong polarity, and the presence of a lone pair results in the formation of complexes with copper, causing severe corrosion of parts made of copper and copper alloys, such as the gaskets of ICEs [8–10].

Detergent-type additives are widely used in the formulation of lubricants for automotive and maritime applications, mainly to keep pistons and other high-temperature surfaces clean of deposits of degradation products [11,12], but also to act as corrosion inhibitors forming a thin self-assembled protective film on metal surfaces, which prevents corrosive molecules from attacking the metal [13–15]. Detergents are composed of an oil-soluble organic and a water-soluble polar head group. The most widely used detergents for this application are sulfonate-, phenate-, and salicylate-type anionic substrates, with calcium as the counterion [13,16]. The inhibition efficiency depends on the film stability, organic molecule structure, and experimental conditions [17].

Since typical lubricant additives have only been tested as corrosion inhibitors for conventional fuels, it is necessary to assess their performance in inhibiting the corrosion of copper by ammonia. In this study, we aim to better understand and classify the performance of the most widely used engine lubricant additives, employing a combination of experiments and computational modeling.

The most accurate computational tools to study chemical systems are ab initio methods, particularly density functional theory (DFT). The use of such methods to study the electronic properties of standalone corrosion inhibitor molecules is nowadays routine, and it can help predict adsorption bonding properties and trends based on the study of HOMO/LUMO orbitals [18]. However, the bonding between the inhibitor molecule and the surface is only one of the many factors affecting the corrosion inhibition performance. The lateral cohesive forces in a film of inhibitor molecules [19,20], and more importantly the diffusivity of the corrosive species through such film [21], are just as important. Studying these properties requires modeling larger systems and long molecular dynamics (MD) trajectories [22], which are out of reach of DFT calculations due to the high computational cost, making it necessary to rely on less-accurate classical force fields.

Several works evaluating the diffusion of corrosive molecules have modeled the inhibitor film as a bulk liquid system, i.e. as a set of

* Corresponding author.
E-mail address: carine.michel@ens-lyon.fr (C. Michel).

https://doi.org/10.1016/j.corsci.2024.112491
Received 30 April 2024; Received in revised form 16 July 2024; Accepted 27 September 2024
Available online 1 October 2024

Table 1
Composition and properties of the oil formulations tested in the experiments.

Name	Additive	%w/w	Kinematic viscosity at 100 °C (mm^2/s)	Kinematic viscosity at 40 °C (mm^2/s)	Viscosity index	Total basic number (mg_{KOH}/g)
			ASTM D7279	ASTM D7279	ISO 2909	ASTM D2896
Oil 1	Sulfonate	10	13.7	124	107	9.8
Oil 2	Phenate	10	15.3	150	103	10.6
Oil 3	Salicylate	10	13.4	123	104	6.5

corrosion inhibitor molecules in a cubic cell with periodic boundary conditions [23–25]. This approach involves disregarding the interactions with the metal surface in which the film is adsorbed. For a representative description of such a film-surface interface, an adequate parametrization of the force fields is required. Parametrization based on experimental information or macroscopic properties has low transferability, since it is not clear how local properties (e.g. conformations) are captured by such models [26], which makes ab initio calculations more attractive reference data for the parametrization. In this sense, we have recently proposed the Gaussian Lennard-Jones (GLJ) approach to describe water/metal interactions [27–29], later extended to describe the chemisorption interaction between oxygen and nitrogen heteroatoms with oxide surfaces [30,31]. The approach involves coupling the long-range attraction and short-range repulsion terms of the Lennard-Jones potential with an additional anisotropic attractive Gaussian potential fitted to data derived from ab initio calculations of small reference molecules containing such heteroatoms. In this way, we can make use of well-established force fields to model the organic molecules and their lateral interactions, while improving the description of their adsorption site and strength on the metal surface [31].

Using the GLJ method we generate models of the corrosion inhibitor films adsorbed on copper. Subsequently, we conduct free energy calculations through thermodynamic integration of molecular dynamics (MD) trajectories to gain insights into the diffusion of ammonia through the films and rationalize these results in terms of the structural properties of the films. Based on our calculations, we identify sulfonates as the best-performing molecules against diffusion of NH_3 towards copper surfaces, which is validated by our corrosion experiments.

2. Methods

2.1. Experiments

The corrosion inhibition performance was evaluated via artificial alteration tests inspired by previous high-temperature alteration methods, developed to study the aging of automotive lubricants [32–34]. The experiments were carried out for three different lubricant oil formulations, all composed of mineral base oils meeting API group II requirements and an additive. The main characteristics of the oils are listed in Table 1. The alteration reaction system consisted of a 2 L custom-made reactor heated to 170 °C via an electrical heating jacket.

The reaction gas mixture was bubbled in the lubricant at a constant total flow rate of 0.85 Nl/min for 100 h, with a magnetic stirrer ensuring the homogeneous distribution of gas bubbles in the oil volume. The reaction gas consisted of a mixture of synthetic air and dry ammonia in stoichiometric composition, corresponding to the contact between the oil film and air/fuel mixture during the intake stroke of a port fuel ammonia engine, and 1000 ppm of nitrogen dioxide, as a potential combustion by-product. Water was also added directly to the oil bulk through a sampling assembly at 0.2 ml/min.

A nitrogen purge flowing above the oil level was applied during ammonia experiments to avoid the concentration of ammonia in the headspace and provide safer experimental conditions. Monitoring of corrosion was conducted using a copper-based corrosion sensor within the alteration reactor, which tracked the material loss of a sacrificial copper layer through capacitive coupling with readout electrodes. The sensor's signal increase served as an indicator of corrosion occurring on the copper surface. The corrosion initiation time (CIT), corresponding to the time when the signal starts to increase, was selected as a descriptor of the corrosion inhibition properties of the lubricant oil. A high CIT value means the onset of copper corrosion is delayed, indicating the lubricant additive is a more effective inhibitor.

Table 2
Fitted parameters for the attractive Gaussian potential for copper-heteroatom (Cu-Het) interactions.

Cu–Het	A (kcal/mol)	b_{xy} ($Å^{-2}$)	b_z ($Å^{-2}$)
Cu–O	−380	1.6	0.65
Cu–N	−800	1.5	0.59

2.2. Molecular mechanics

Molecular mechanics calculations were carried out using a modified version of CP2K 9.1 [35]. Long-range Coulombic interactions were evaluated by smooth particle-mesh Ewald summation [36] with a width parameter of 0.36 $Å^{-1}$ and a grid of about 1 point per Å of the corresponding unit-cell length. Standard scaling factors of 0.5 and 0.833 were used for van der Waals and electrostatic 1–4 interaction respectively. Organic molecules were modeled with the General AMBER Force Field [37,38], using the AM1-BCC charge method [39], and Lorentz/Berthelot combination rules for interactions between different atom types, as implemented in the Antechamber package of AmberTools [40]. The divalent Ca cations were modeled using the 12-6 LJ-type parameters of Li and Merz [41,42].

The Lennard-Jones parameters derived by Heinz et al. [43] were employed to model the copper surface. To enhance the interfacial interactions with the polar heads, we included anisotropic attractive Gaussian potentials between the copper surface atoms and the heteroatoms (Het) of the organic molecules that interact strongly with the metal surface (N or O), as we have done in a previous work to describe Al–O, Al–N, Fe–O and Fe–N interactions [30]. The attractive potentials are described as follows:

$$V_{\mathrm{Cu-Het}}(r_{xy}, r_z) = A e^{-b_{xy} r_{xy}^2} e^{-b_z r_z^2} \quad (1)$$

where A is the magnitude of the Gaussian attraction, r_{xy} and r_z are the Cu–Het distances in the xy plane and the out-of-plane z direction, respectively, and b_{xy} and b_z are the corresponding width parameters of the Gaussian function. The Gaussian potentials of Cu–O and Cu–N were parameterized based on reference data derived from DFT calculations. The inclusion of these attractive Gaussian potentials improves the corrugation of the interfacial potential when the diffusion of the organic molecule parallel to the surface is considered, as shown in Figure S1. In particular, the correct site-preference (top) of hetero-atoms is restored by the attractive Gaussian potential, while the LJ potential inevitably leads to preferred hollow adsorption sites. The final 6 parameters are provided in Table 2.

The copper surface was modeled as Cu(111), the most stable low-index termination. A 4-layer $3\sqrt{3}\times3\sqrt{3}$ slab was cleaved from the fcc Cu bulk, optimized via DFT with relaxation of the two uppermost layers, and used for the fitting of the anisotropic Gaussian potential. Subsequently, a $6\sqrt{3}\times6\sqrt{3}$ slab (6.25 nm^2) with 108 Cu atoms per layer was derived from the DFT-optimized one, and used in the classical force field calculations, keeping the coordinates of all Cu atoms fixed.

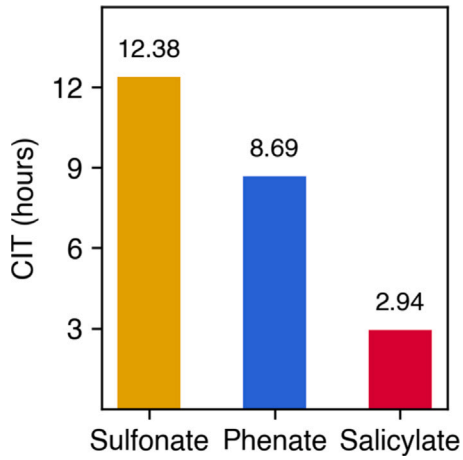

Fig. 1. Corrosion initiation time (CIT) measured in the alteration experiments for the three oil formulations evaluated, labeled according to the additive used in each of them.

The geometry of the films was optimized using the limited memory BFGS (LBFGS) method as implemented in CP2K,[44] prior to the molecular dynamics (MD) simulations.

In all MD simulations, a time step of 0.5 fs was used, and the NVT ensemble was selected, using a Nose–Hoover thermostat (T = 423 K), with a time constant of 200 fs. For the equilibration of the films, we carried out MD simulations of 1 ns, obtaining statistical data on the structure of the films. Subsequently, to study the diffusion of ammonia through the film, an NH_3 molecule was placed outside of the film with nitrogen at a distance of 30.5 Å from the uppermost copper layer, with an equivalent system generated for the clean Cu surface as well, as a blank reference. For each system, we carried out MD simulations for 290 ps, setting the z coordinate of the nitrogen atom in NH_3 as a collective variable, and imposing a constraint to evolve the distance to the surface from 30.5 Å to 1.5 Å at a rate of 0.1 Å/ps. Then, MD simulations of 800 ps were run for selected frames of the resulting trajectory, modifying the constraint to keep the z coordinate of nitrogen fixed, and recording the Lagrange multiplier of this constraint, which is equivalent to the force exerted on the nitrogen atom when fixed at that particular distance from the surface [45]. The average force $\langle F \rangle$ was evaluated in the range of 300–800 ps (i.e. discarding the first 300 ps of equilibration).

3. Results and discussion

We have assessed the copper corrosion inhibition efficiency of three additives typically present in commercial engine lubricants, namely sulfonates, phenates, and salicylates. In Section 3.1 we briefly present the experimental results used as a reference, against which we validate the simulations. In Section 3.2 we describe the generation of the film models via molecular dynamics. We used the GLJ method, which provides a better description of the chemisorption interaction of oxygen and nitrogen with the surface and allows for a correct prediction of their preferred adsorption site. In Section 3.3 we study the free energy of diffusion of an ammonia molecule through the film, which serves as a descriptor of the corrosion inhibitor efficiency, since a higher diffusion barrier decreases the probability of corrosive molecules reaching the metal surface. Finally, in Section 3.4 we discuss possible explanations for the results obtained based on the analysis of the structural properties of the films.

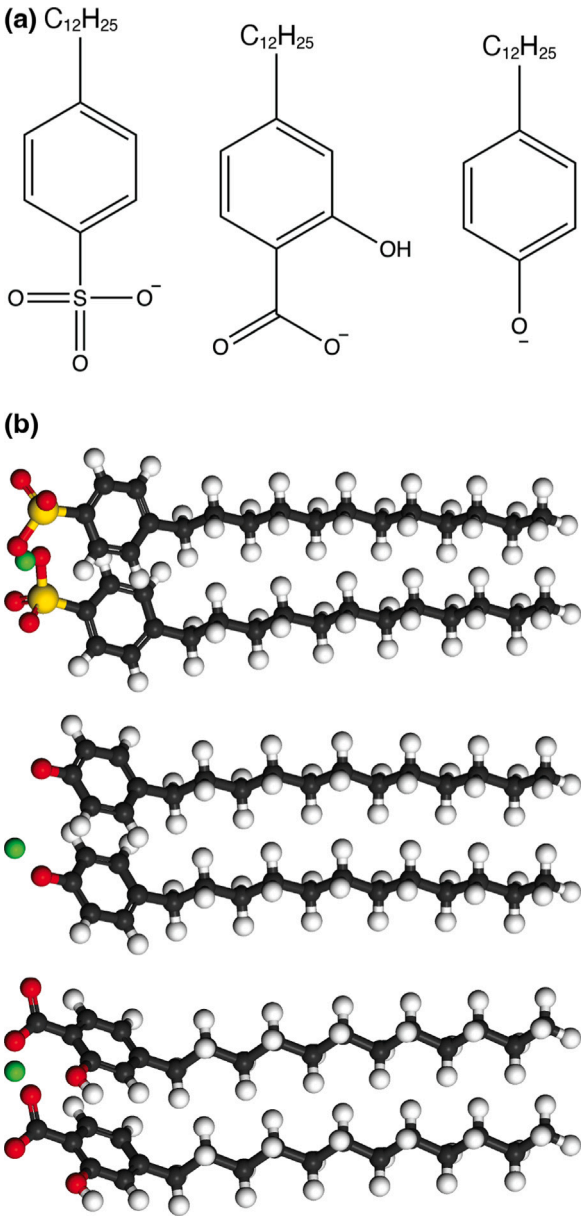

Fig. 2. (a) Chemical structures of (from left to right) sulfonate, phenate and salicylate anions used as corrosion inhibitors (b) Ball and stick representation of the complete molecules used in the simulation of the films (same order from top to bottom). Carbon in black, hydrogen in white, oxygen in red, sulfur in yellow, calcium in green. (For interpretation of the references to color in this figure legend, the reader is referred to the web version of this article.)

3.1. Corrosion inhibition experiments

Each of the three oil formulations considered contain a different additive: sulfonate, phenate, or salicylate, all at equal concentration, enabling a comparison of their performance as corrosion inhibitors.

Fig. 1 presents the corrosion initiation time (CIT) measured in the alteration experiments for each lubricant oil formulation. We find that salicylate exhibits the lowest protection against ammonia corrosion, with a CIT of just under 3 h. On the other hand, the sulfonate additive provides the highest protection, allowing for a CIT of over 12 h. Finally, the oil formulation using a phenate additive lies in between, with a CIT close to 9 h. These results suggest that at iso-concentration sulfonate is the most effective corrosion inhibition additive for ammonia engines.

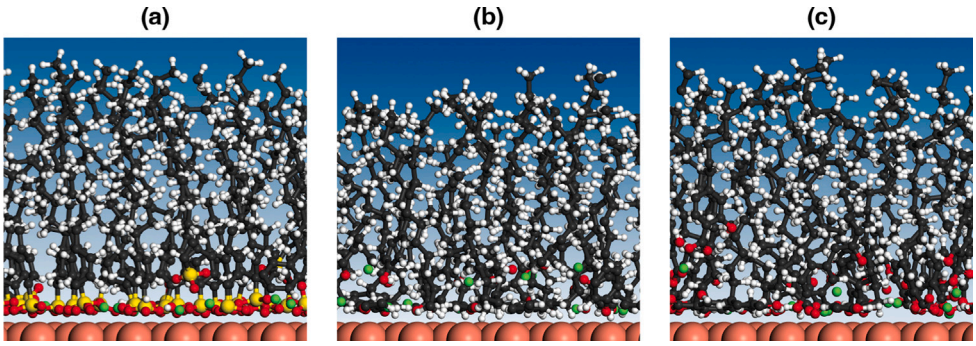

Fig. 3. Typical structure of the corrosion inhibitor films on Cu(111), (a) Sulfonate, (b) Phenate (c) Salicylate. Carbon in black, hydrogen in white, oxygen in red, sulfur in yellow, calcium in green, and copper in brown. (For interpretation of the references to color in this figure legend, the reader is referred to the web version of this article.)

3.2. Simulation of the inhibitor films

The sulfonate, phenate, and salicylate molecules consist of alkyl benzene ligands with polar $–SO_3^-$, $–O^-$, and –COOH substituents, respectively, bound to the aromatic ring (Fig. 2a). The length of the alkyl chain was set to 12 carbon atoms, since dodecylbenzene is the most common alkylbenzene used for the production of the corresponding sulfonate [13]. Charge neutrality is achieved by adding one calcium cation for every two anionic ligands (Fig. 2b).

The initial placement of the ligands on the surface of the calculation slab was obtained using the Packmol package [46], with coverages of 24, 26, and 28 ligands for salicylate, sulfonate, and phenate, respectively. These values represent the maximum coverages for which desorption is not observed during the equilibration calculations described in Section 2.2. It is worth noting that attempting to match the concentration in the experimental solution would be inaccurate, since for exergonic adsorption in equilibrium, the concentration of ligands at the surface should be higher than in the bulk oil [18]. To improve the sampling, we generated and equilibrated three different films for each type of ligand. Fig. 3 illustrates the morphology of the three systems after equilibration.

3.3. Diffusion of ammonia

To evaluate the corrosion inhibition efficiency we calculated the free energy profiles of NH_3 diffusion towards the Cu(111) surface through the films via thermodynamic integration. For each of the 3 different films that we had generated per ligand, we repeated the aforementioned procedure 3 times using different random initial velocities, obtaining a total of 9 sets of data points per ligand, each of them establishing a function between the average force acting on the nitrogen atom and its z coordinate. These sets were averaged to obtain a final representative relationship between the force and the distance of ammonia to the surface. The raw data including the standard deviation is presented in Tables S1–S3 in the Supporting Information.

The free energy profile associated with the interaction between NH_3 and the films was obtained via the integration of the average forces $\langle F(z')\rangle$:

$$\Delta G(z) = -\int_{\text{outside}}^{z} \langle F(z')\rangle \, dz'$$

The free energy profiles for the interaction of NH_3 with the clean Cu surface and with the three films are presented in Fig. 4 and in Figure S3 showing the confidence intervals.

For the clean Cu(111) surface, the free energy profile reflects the interaction potential between NH_3 and the surface, which is given by the sum of the contributions of Lennard-Jones and Gaussian potentials. The resulting free energy profile displays a minimum of −71 kJ/mol at a distance of 2.5 Å from the surface, corresponding to the adsorption of NH_3. The free energy approaches zero as the molecule moves away from the surface, while it rapidly becomes positive (repulsive interaction) when moving closer to the surface.

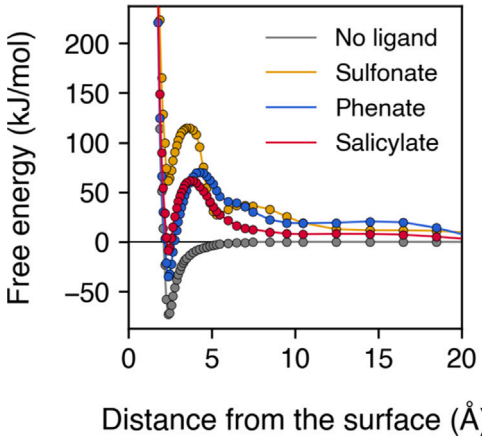

Fig. 4. Free energy profiles for the diffusion of an NH_3 molecule towards the Cu(111) surface. For each system the zero is set outside of the films and 30.5 Å away from the surface.

In the case of the corrosion inhibitor films, the free energy remains low as NH_3 approaches the surface until reaching a distance of about 8 Å to the surface, even though the films extend up to about 22 Å from the surface. This indicates that NH_3 can easily penetrate the alkyl tail of the films. At distances closer than 8 Å an energy barrier appears in all cases, which roughly matches the average location of the ligand heads (e.g. 7.4 Å for the upper carbon of the aromatic ring in sulfonate films). The highest energy barrier is observed for the case of sulfonates, with a maximum of 115 kJ/mol at 3.7 Å from the surface. Moreover, the local adsorption minimum found at 2.4 Å is higher in free energy (+62 kJ/mol) than the reference state where NH_3 is outside of the film. In other words, the adsorption of NH_3 is endergonic, which prevents corrosion. Phenate and salicylate films present lower free energy barriers, of 70 and 63 kJ/mol respectively. Furthermore, in both cases the adsorption of NH_3 is exergonic, although less than on the clean surface, with free energies of −35 kJ/mol for phenate and −6 kJ/mol for salicylate.

Overall, the calculated free energy profiles show excellent agreement with the corrosion initiation time experiments, indicating that the three types of corrosion inhibitor films studied can be ranked, in terms of their ability to prevent the diffusion of NH_3 towards the metal surface, as follows: sulfonate > phenate > salicylate.

3.4. Analysis of the structure of the films

To understand and rationalize the corrosion inhibition performance of the films, we evaluated their structural properties averaged over the

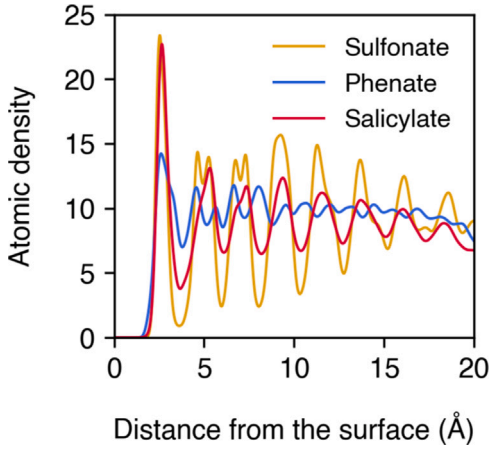

Fig. 5. Atomic density of the films as a function of the distance to the Cu(111) surface.

equilibration trajectories. In this analysis, the first 0.5 ns of the MD simulations were discarded as thermalization points, and only subsequent points were considered for the calculation of average properties.

We observe that the three films present similar average thickness, calculated as the distance between the atoms positioned farthest and closest to the surface. The thickness values are 21.7, 23.2, and 21.8 Å for sulfonate, phenate, and salicylate, respectively.

The global atomic density as a function of the distance to the surface was determined via kernel density estimation, using a Gaussian distribution with a width of 0.2 (Fig. 5). The integral of the atomic density in z gives the total number of atoms in the films. In this sense, it is worth noting that the total number of ligands differs, as well as the total number of atoms per ligand, since sulfonate and salicylate have both 103 atoms (including the Ca cation), whereas phenate has only 97 atoms.

We observe that all films have a maximum atomic density very close to the surface, at a distance of about 2.6 Å, which coincides with the statistical mode of the position of the Ca cations in the films. However, after the first peak, sulfonate seems to preserve a well-ordered structure in the z direction, perpendcular to the interface, characterized by marked hills and valleys in the atomic density profile, which contrasts with the relatively smoother atomic density of salicylate, and the clearly disordered profile of phenate. This is also reflected in the distribution of Ca cations. In the sulfonate film, all Ca cations are located close to the surface, with an average distance of 2.60 ± 0.17 Å. The low standard deviation indicates a consistent adsorption structure for all ligands. In contrast, salicylate and phenate films show larger deviations, with some Ca cations straying away from the surface, resulting in average distances of 2.81 ± 0.45 Å and 4.17 ± 1.83 Å, respectively. The difference likely arises from the tridentate adsorption of sulfonate, which covers the surface with negative charges trapping the Ca cations nearby.

We can also understand the film's ordering by looking at the distribution of tilt angles of the ligand heads with respect to the surface normal (Fig. 6). The angle measured was the one delimited by a vector formed between the atom of the polar head immediately bound to the aromatic ring (oxygen in phenate, carbon in salicylate, and sulfur in sulfonate), and the carbon atom in the para position of the aromatic ring. We observe that the sulfonate film has a narrow distribution, with a statistical mode of 11 degrees and an average of 16 degrees, corresponding to a film almost perpendicular to the surface. Salicylate also has a mode of 11 degrees, but the distribution comprises a wider range of tilt angles, shifting the average value to 31 degrees, and incorporating a significant amount of flat (angle of 90 degrees) ligands. Finally, phenate presents mode and average tilt angles of 42 and 44 degrees, with a significant number of ligand heads adsorbed flat on the surface as well. The narrower distribution of sulfonate reflects its higher degree of ordering.

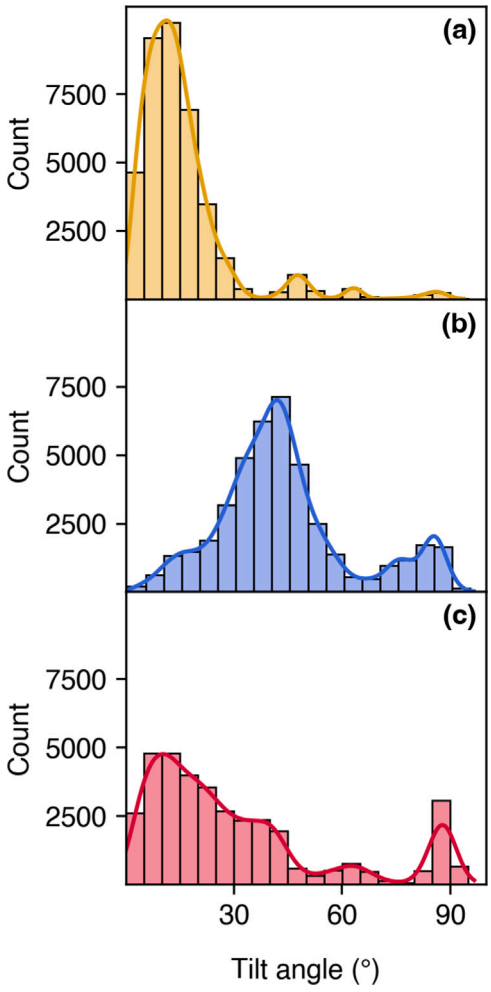

Fig. 6. Tilt angle of the polar heads of corrosion inhibitor molecules on Cu(111) with respect to the surface normal (i.e. 90° corresponds to flat adsorption). (a) Sulfonate, (b) Phenate (c) Salicylate.

Finally, a third molecular-scale variable that can be associated with the diffusion of molecules through films is the fractional free volume (FFV) [23–25,47], calculated as the free volume (V_f) divided by the total volume of the cell.

$$FFV = \frac{V_f}{V_{tot}} 100\% \quad (2)$$

Large openings in the inhibitor film result in higher FFV, facilitating the diffusion of NH_3, and thus lowering the inhibition efficiency [48,49]. The free and occupied volumes inside the calculation cell were obtained using the Connolly surface algorithm as implemented in the BIOVIA Materials Studio software. The Connolly surface is calculated as the surface defined by a probe of 1.63 Å of radius (molecular radius of NH_3 [50]) rolling over the van der Waals surface formed by the atoms of the film. In this way, small voids inaccessible for NH_3 molecules are not counted in the free volume. To obtain more representative numbers, the trivial free volume over 30 Å away from the surface (never accessed by the films) was subtracted from the total free volume. Similarly, the volume corresponding to the Cu surface slab was subtracted from the occupied volume. This analysis was performed for 3 points along the equilibration trajectory of the 3 films generated for each ligand, giving a total of 9 FFV values per ligand, from which we obtain average values. Our results indicate that the sulfonate film

Table 3
Summary of the results. Experimental corrosion initiation time (CIT), free energy barrier for the diffusion of NH_3, mode and average of the tilt angle, and fractional free volume of the films.

Ligand	CIT (h)	ΔG barrier (kJ/mol)	Mode tilt angle	Average tilt angle	FFV (%)
Sulfonate	12.38	115	11	16	2.2 ± 0.7
Phenate	8.69	70	42	44	5.8 ± 0.3
Salicylate	2.94	63	11	31	11.0 ± 0.9

presents the lowest FFV, with an average of 2.2 ± 0.7%, followed by phenate and salicylate with FFV of 5.8 ± 0.3% and 11.0 ± 0.9%, respectively. Sulfonate having the lowest FFV indicates that it should present the highest opposition towards ammonia diffusion, in good agreement with the trends in the diffusion barrier (Fig. 4), as well as with the experimental results.

Table 3 provides a summary of the results for each of the three corrosion inhibitor molecules studied, comparing the results of the experimental analysis and the three main computational descriptors evaluated.

4. Conclusions

In summary, we have employed a classical force field coupled with an anisotropic Gaussian potential to simulate the diffusion of ammonia through detergent-based films of calcium sulfonate, phenate, and salicylate adsorbed on copper. Our findings indicate that sulfonate opposes the highest energy barrier towards ammonia diffusion, which makes it an effective corrosion inhibitor by preventing the interaction between ammonia and the copper surface. Phenate and salicylate present lower energy barriers and therefore are less effective. These results are in very good agreement with our corrosion inhibition experiments, which show that lubricant oils containing a sulfonate additive provide the longest protection of the copper sensor against gaseous ammonia.

The effectiveness of sulfonate may be attributed to its well-ordered structure compared to the other two types of films, as evidenced by its atomic density profile and narrow distribution of ligand tilt angles. Furthermore, the ability of a film to restrict the diffusion of ammonia is also correlated with the fractional free volume (FFV) available. Our models are consistent with this descriptor, as sulfonate presents the lowest fractional free volume among the three types of films. The agreement of the FFV with the free energy profiles suggests that it could be a promising method for quickly screening corrosion inhibitors, as its evaluation is straightforward and computationally inexpensive. However, molecular models of the films are still required for this type of analysis. To further advance the rational design of corrosion inhibitors it is thus necessary to gain insight into the relationship between the characteristics of individual molecules and the properties of the films they form.

Overall, we have developed a computational protocol to assess the performance of corrosion inhibitor films. We identify the free energy of ammonia diffusion and the fractional free volume of the film as good descriptors of corrosion inhibition efficiency, providing good qualitative agreement with experiments. This protocol is a promising approach for screening novel or modified formulations of corrosion inhibitor additives.

CRediT authorship contribution statement

Agustin Salcedo: Writing – original draft, Visualization, Software, Methodology, Formal analysis, Data curation. **Stefano Caputo:** Visualization, Methodology. **Sophie Loehlé:** Writing – review & editing, Supervision, Resources, Project administration, Conceptualization. **Stephan N. Steinmann:** Writing – review & editing, Writing – original draft, Validation, Supervision, Methodology, Formal analysis, Conceptualization. **Carine Michel:** Writing – review & editing, Validation, Supervision, Resources, Project administration, Conceptualization.

Declaration of competing interest

The authors declare the following financial interests/personal relationships which may be considered as potential competing interests: Carine MICHEL reports financial support was provided by Total Energy Services Inc. If there are other authors, they declare that they have no known competing financial interests or personal relationships that could have appeared to influence the work reported in this paper.

Data availability

We have shared example CP2K input files to reproduce the simulations.

Acknowledgments

The authors acknowledge the PSMN mesocenter in Lyon for CPU time and assistance (CPER/SYSPROD 2015–2022 project No. 2019-AURA-P5B and AXELERA Pôle de compétitivité). Experiments were partially realized in research projects with financial support from the participating project partners and the Austrian COMET program (Project InTribology, No. 872176) at AC2T research GmbH. The authors wish to acknowledge the laboratory AC2T research GmbH for their contribution to the development of the artificial alteration method A. Agocs and C. Besser. The authors thank Maria Rappo and Bruno Griffaton for fruitful discussions.

Appendix A. Supplementary data

Supplementary material related to this article can be found online at https://doi.org/10.1016/j.corsci.2024.112491.

References

[1] M.-C. Chiong, H.-S. Kang, N.M.R. Shaharuddin, S. Mat, L.K. Quen, K.-H. Ten, M.C. Ong, Challenges and opportunities of marine propulsion with alternative fuels, Renew. Sustain. Energy Rev. 149 (2021) 111397, http://dx.doi.org/10.1016/j.rser.2021.111397.

[2] F.Y. Al-Aboosi, M.M. El-Halwagi, M. Moore, R.B. Nielsen, Renewable ammonia as an alternative fuel for the shipping industry, Curr. Opin. Chem. Eng. 31 (2021) 100670, http://dx.doi.org/10.1016/j.coche.2021.100670.

[3] C. Kurien, M. Mittal, Review on the production and utilization of green ammonia as an alternate fuel in dual-fuel compression ignition engines, Energy Convers. Manage. 251 (2022) 114990, http://dx.doi.org/10.1016/j.enconman.2021.114990.

[4] A. Boretti, S. Castelletto, NH_3 prospects in combustion engines and fuel cells for commercial aviation by 2030, ACS Energy Lett. 7 (2022) 2557–2564, http://dx.doi.org/10.1021/acsenergylett.2c00994.

[5] H. Kobayashi, A. Hayakawa, K.D.K.A. Somarathne, E.C. Okafor, Science and technology of ammonia combustion, Proc. Combust. Inst. 37 (2019) 109–133, http://dx.doi.org/10.1016/j.proci.2018.09.029.

[6] A.M. Elbaz, S. Wang, T.F. Guiberti, W.L. Roberts, Review on the recent advances on ammonia combustion from the fundamentals to the applications, Fuel Commun. 10 (2022) 100053, http://dx.doi.org/10.1016/j.jfueco.2022.100053.

[7] P. Dimitriou, R. Javaid, A review of ammonia as a compression ignition engine fuel, Int. J. Hydrog. Energy 45 (2020) 7098–7118, http://dx.doi.org/10.1016/j.ijhydene.2019.12.209.

[8] M.-K. Hsieh, D.A. Dzombak, R.D. Vidic, Effect of tolyltriazole on the corrosion protection of copper against ammonia and disinfectants in cooling systems, Ind. Eng. Chem. Res. 49 (2010) 7313–7322, http://dx.doi.org/10.1021/ie100384d.

[9] R. Francis, The Corrosion of Copper and Its Alloys: A Practical Guide for Engineers, NACE International, 2010.

[10] C. Tornatore, L. Marchitto, P. Sabia, M.D. Joannon, Ammonia as green fuel in internal combustion engines: State-of-the-art and future perspectives, Front. Mech. Eng. 8 (2022) http://dx.doi.org/10.3389/fmech.2022.944201.
[11] U. Zoller, in: U. Zoller (Ed.), Handbook of Detergents, Part E, CRC Press, 2008, http://dx.doi.org/10.1201/9781420018165.
[12] A.M. Nassar, N.S. Ahmed, R.I. El-shazly, Y.K.A. el menem, Preparation and evaluation of the mixtures of sulfonate and phenate as lube oil additives, Int. J. Ind. Chem. 8 (2017) 383–395, http://dx.doi.org/10.1007/s40090-017-0128-x.
[13] S.P. O'Connor, J. Crawford, C. Cane, Overbased lubricant detergents – a comparative study, Lubr. Sci. 6 (1994) 297–325, http://dx.doi.org/10.1002/ls.3010060402.
[14] A.B. Vipper, S.J. Cook, A.K. Karaulov, R. Leahy, Antifriction properties of calcium phenate-type detergents used in marine cylinder lubricants, Lubr. Sci. 10 (1998) 163–170, http://dx.doi.org/10.1002/ls.3010100206.
[15] J. Mathiyarasu, S.S. Pathak, V. Yegnaraman, Review on corrosion prevention of copper using ultrathin organic monolayers, Corros. Rev. 24 (2006) http://dx.doi.org/10.1515/CORRREV.2006.24.5-6.307.
[16] E. Seddon, C. Friend, J. Roski, Detergents and dispersants, Springer Netherlands, Dordrecht, 2009, pp. 213–236, http://dx.doi.org/10.1023/b105569,
[17] Y.S. Tan, M.P. Srinivasan, S.O. Pehkonen, S.Y.M. Chooi, Self-assembled organic thin films on electroplated copper for prevention of corrosion, J. Vacuum Sci. Technol. A: Vacuum Surf. Films 22 (2004) 1917–1925, http://dx.doi.org/10.1116/1.1763901.
[18] A. Kokalj, Molecular modeling of organic corrosion inhibitors: Calculations, pitfalls, and conceptualization of molecule–surface bonding, Corros. Sci. 193 (2021) 109650, http://dx.doi.org/10.1016/j.corsci.2021.109650.
[19] S. Ramachandran, B.-L. Tsai, M. Blanco, H. Chen, Y. Tang, W.A. Goddard, Self-assembled monolayer mechanism for corrosion inhibition of iron by imidazolines, Langmuir 12 (1996) 6419–6428, http://dx.doi.org/10.1021/la960646y.
[20] M. Poberžnik, F. Chiter, I. Milošev, P. Marcus, D. Costa, A. Kokalj, DFT study of n-alkyl carboxylic acids on oxidized aluminum surfaces: From standalone molecules to self-assembled-monolayers, Appl. Surf. Sci. 525 (2020) 146156, http://dx.doi.org/10.1016/j.apsusc.2020.146156.
[21] A. Kokalj, D. Costa, Model study of penetration of Cl^- ions from solution into organic self-assembled-monolayer on metal substrate: Trends and modeling aspects, J. Electrochem. Soc. 168 (2021) 071508, http://dx.doi.org/10.1149/1945-7111/ac0a24.
[22] C. Verma, H. Lgaz, D. Verma, E.E. Ebenso, I. Bahadur, M. Quraishi, Molecular dynamics and Monte Carlo simulations as powerful tools for study of interfacial adsorption behavior of corrosion inhibitors in aqueous phase: A review, J. Mol. Liq. 260 (2018) 99–120, http://dx.doi.org/10.1016/j.molliq.2018.03.045.
[23] J. Zhang, W. Yu, L. Yu, Y. Yan, G. Qiao, S. Hu, Y. Ti, Molecular dynamics simulation of corrosive particle diffusion in benzimidazole inhibitor films, Corros. Sci. 53 (2011) 1331–1336, http://dx.doi.org/10.1016/j.corsci.2010.12.027.
[24] Y. Yan, X. Wang, Y. Zhang, P. Wang, X. Cao, J. Zhang, Molecular dynamics simulation of corrosive species diffusion in imidazoline inhibitor films with different alkyl chain length, Corros. Sci. 73 (2013) 123–129, http://dx.doi.org/10.1016/j.corsci.2013.03.031.
[25] Q. Zhang, Y. Li, G. Zhu, Y. Lei, X. Wang, H. Liu, G. Zhang, In-depth insight into the synergistic inhibition mechanism of S-benzyl-L-cysteine and thiourea on the corrosion of carbon steel in the CO_2-saturated oilfield produced water, Corros. Sci. 192 (2021) 109807, http://dx.doi.org/10.1016/j.corsci.2021.109807.
[26] C.R. Herbers, C. Li, N.F.A. van der Vegt, Grand challenges in quantum-classical modeling of molecule–surface interactions, J. Comput. Chem. 34 (2013) 1177–1188, http://dx.doi.org/10.1002/jcc.23247.
[27] S.N. Steinmann, R.F.D. Morais, A.W. Götz, P. Fleurat-Lessard, M. Iannuzzi, P. Sautet, C. Michel, Force field for water over Pt(111): Development, assessment, and comparison, J. Chem. Theory Comput. 14 (2018) 3238–3251, http://dx.doi.org/10.1021/acs.jctc.7b01177.
[28] P. Clabaut, P. Fleurat-Lessard, C. Michel, S.N. Steinmann, Ten facets, one force field: The GAL19 force field for water–noble metal interfaces, J. Chem. Theory Comput. 16 (2020) 4565–4578, http://dx.doi.org/10.1021/acs.jctc.0c00091.
[29] P. Clabaut, M. Beisert, C. Michel, S.N. Steinmann, Beyond single-crystal surfaces: The GAL21 water/metal force field, J. Chem. Phys. 157 (2022) http://dx.doi.org/10.1063/5.0130368.
[30] J. Rey, S. Blanck, P. Clabaut, S. Loehlé, S.N. Steinmann, C. Michel, Transferable Gaussian attractive potentials for organic/oxide interfaces, J. Phys. Chem. B 125 (2021) 10843–10853, http://dx.doi.org/10.1021/acs.jpcb.1c05156.
[31] X. Wu, S.N. Steinmann, C. Michel, Gaussian attractive potential for carboxylate/cobalt surface interactions, J. Chem. Phys. 159 (2023) http://dx.doi.org/10.1063/5.0173351.
[32] CEC, L-48-A00: Oxidation stability of lubricating oils used in automotive transmissions by artificial ageing, 2007, Coordinating European Council for the Development of Performance Tests for Fuels, Lubricants and Other Fluids.
[33] C. Besser, C. Schneidhofer, N. Dörr, F. Novotny-Farkas, G. Allmaier, Investigation of long-term engine oil performance using lab-based artificial ageing illustrated by the impact of ethanol as fuel component, Tribol. Int. 46 (2012) 174–182, http://dx.doi.org/10.1016/j.triboint.2011.06.026.
[34] C. Besser, A. Agocs, B. Ronai, A. Ristic, M. Repka, E. Jankes, C. McAleese, N. Dörr, Generation of engine oils with defined degree of degradation by means of a large scale artificial alteration method, Tribol. Int. 132 (2019) 39–49, http://dx.doi.org/10.1016/j.triboint.2018.12.003.
[35] J. Hutter, M. Iannuzzi, F. Schiffmann, J. VandeVondele, Cp2k: atomistic simulations of condensed matter systems, Wiley Interdiscip. Rev.: Comput. Mol. Sci. 4 (2014) 15–25, http://dx.doi.org/10.1002/wcms.1159.
[36] U. Essmann, L. Perera, M.L. Berkowitz, T. Darden, H. Lee, L.G. Pedersen, A smooth particle mesh Ewald method, J. Chem. Phys. 103 (1995) 8577–8593, http://dx.doi.org/10.1063/1.470117.
[37] J. Wang, R.M. Wolf, J.W. Caldwell, P.A. Kollman, D.A. Case, Development and testing of a general amber force field, J. Comput. Chem. 25 (2004) 1157–1174, http://dx.doi.org/10.1002/jcc.20035.
[38] J. Wang, W. Wang, P.A. Kollman, D.A. Case, Automatic atom type and bond type perception in molecular mechanical calculations, J. Mol. Graph. Model. 25 (2006) 247–260, http://dx.doi.org/10.1016/j.jmgm.2005.12.005.
[39] A. Jakalian, D.B. Jack, C.I. Bayly, Fast, efficient generation of high-quality atomic charges. AM1-BCC model: II. Parameterization and validation, J. Comput. Chem. 23 (2002) 1623–1641, http://dx.doi.org/10.1002/jcc.10128.
[40] D.A. Case, D. Cerutti, T.E. Cheatham III, T.A. Darden, R.E. Duke, T.J. Giese, H. Gohlke, A.W. Goetz, D. Greene, N. Homeyer, S. Izadi, A. Kovalenko, T.S. Lee, S. LeGrand, P. Li, C. Lin, J. Liu, T. Luchko, R. Luo, D. Mermelstein, K.M. Merz, G. Monard, H. Nguyen, I. Omelyan, A. Onufriev, F. Pan, R. Qi, D.R. Roe, A. Roitberg, C. Sagui, C.L. Simmerling, W.M. Botello-Smith, J. Swails, R.C. Walker, J. Wang, R.M. Wolf, X. Wu, L. Xiao, D.M. York, P.A. Kollman, AMBER2017, 2017.
[41] P. Li, K.M. Merz, Taking into account the ion-induced dipole interaction in the nonbonded model of ions, J. Chem. Theory Comput. 10 (2014) 289–297, http://dx.doi.org/10.1021/ct400751u.
[42] Z. Li, L.F. Song, P. Li, K.M. Merz, Systematic parametrization of divalent metal ions for the OPC3, OPC, TIP3P-FB, and TIP4P-FB water models, J. Chem. Theory Comput. 16 (2020) 4429–4442, http://dx.doi.org/10.1021/acs.jctc.0c00194.
[43] H. Heinz, R.A. Vaia, B.L. Farmer, R.R. Naik, Accurate simulation of surfaces and interfaces of face-centered cubic metals using 12-6 and 9-6 Lennard–Jones potentials, J. Phys. Chem. C 112 (2008) 17281–17290, http://dx.doi.org/10.1021/jp801931d.
[44] R.H. Byrd, P. Lu, J. Nocedal, C. Zhu, A limited memory algorithm for bound constrained optimization, SIAM J. Sci. Comput. 16 (1995) 1190–1208, http://dx.doi.org/10.1137/0916069.
[45] E. Carter, G. Ciccotti, J.T. Hynes, R. Kapral, Constrained reaction coordinate dynamics for the simulation of rare events, Chem. Phys. Lett. 156 (5) (1989) 472–477, http://dx.doi.org/10.1016/S0009-2614(89)87314-2.
[46] L. Martínez, R. Andrade, E.G. Birgin, J.M. Martínez, PACKMOL: A package for building initial configurations for molecular dynamics simulations, J. Comput. Chem. 30 (2009) 2157–2164, http://dx.doi.org/10.1002/jcc.21224.
[47] F. Pan, F. Peng, Z. Jiang, Diffusion behavior of benzene/cyclohexane molecules in poly(vinyl alcohol)-graphite hybrid membranes by molecular dynamics simulation, Chem. Eng. Sci. 62 (2007) 703–710, http://dx.doi.org/10.1016/j.ces.2006.07.046.
[48] S.-Q. Hu, A.-L. Guo, Y.-G. Yan, X.-L. Jia, Y.-F. Geng, W.-Y. Guo, Computer simulation of diffusion of corrosive particle in corrosion inhibitor membrane, Comput. Theor. Chem. 964 (2011) 176–181, http://dx.doi.org/10.1016/j.comptc.2010.12.019.
[49] H. Lgaz, R. Salghi, S. Masroor, S.-H. Kim, C. Kwon, S.Y. Kim, Y.-J. Yang, I.-M. Chung, Assessing corrosion inhibition characteristics of hydrazone derivatives on mild steel in HCl: Insights from electronic-scale DFT and atomic-scale molecular dynamics, J. Mol. Liq. 308 (2020) 112998, http://dx.doi.org/10.1016/j.molliq.2020.112998.
[50] M. Kanezashi, A. Yamamoto, T. Yoshioka, T. Tsuru, Characteristics of ammonia permeation through porous silica membranes, AIChE J. 56 (2010) 1204–1212, http://dx.doi.org/10.1002/aic.12059.